Environmental Science Nano

ROYAL SOCIETY OF CHEMISTRY

PAPER

View Article Online
View Journal | View Issue

Check for updates

Cite this: *Environ. Sci.: Nano*, 2026, **13**, 1700

Unravelling the role of nanoparticle morphology during uptake and transport in eggplants

Lifei Xi, [ab] Yamin Wang, [b] Alfiz Muhammad Qizwini,[b] Yee Yan Tay,[a] Chris Boothroyd[ab] and Yeng Ming Lam *[ab]

Received 1st October 2025,
Accepted 18th February 2026

DOI: 10.1039/d5en00920k

rsc.li/es-nano

Understanding how the morphology of nanocarriers influences their interaction with plants is crucial for assessing their impact on plant health, human safety, and the environment, as well as exploring their potential applications in environmental remediation, plant sensing, and target delivery in plants. In this study, we designed and synthesized hydrophilic gold (Au) nanospheres and nanowires encapsulated in beta-cyclodextrin (β-CD) polymer as target nutrient carriers, and studied their translocation in eggplants. Electron microscopy and elemental analysis reveal that both nanocarrier types can penetrate the leaf surface, redistribute within leaf tissues, and undergo long-distance transport to stems and roots *via* vascular-associated pathways. Distinct morphology-dependent behaviour is observed: spherical nanocarriers largely retain their shape during transport, whereas wire-shaped nanocarriers frequently appear as fragmented segments within plant tissues. Given the low fraction of nanospheres in the initial suspension, this observation indicates in planta transformation rather than selective uptake of pre-existing fragments. Nanocarriers are predominantly localised in cell walls, intercellular spaces, and phloem-associated regions, with roots acting as terminal compartments for accumulation or exclusion of non-essential elements. Together, these results demonstrate that nanocarrier morphology influences both structural stability and spatial distribution in plants following foliar exposure. While the underlying molecular transport mechanisms remain to be fully resolved, this study provides experimentally supported insights into morphology-dependent nanocarrier behaviour and offers a framework for the future design of plant-compatible nanocarrier systems.

Environmental significance

The application of nanotechnology in agriculture offers opportunities for improving nutrient delivery and reducing chemical waste but understanding how nanocarriers interact with plants is essential to ensure environmental safety. Current knowledge gaps on nanoparticle uptake and movement within plants limit both risk assessment and technological advancement. In this work, we show that hydrophilic gold nanospheres and nanowires encapsulated in beta-cyclodextrin (β-CD) polymer can penetrate the cuticle, translocate through leaf tissues, and accumulate in roots *via* the vascular system. Importantly, nanowires disintegrate into smaller fragments during transport, highlighting the role of physical and chemical forces. These findings provide critical insights for developing sustainable nanocarrier-based agricultural practices with minimized ecological risks.

1. Introduction

In recent years, nanotechnology has emerged as a promising strategy to deliver specialty agrochemicals precisely into subcellular compartments in plants and to control the amount of nutrients delivered accurately.[1–4] It is found that the size, shape, surface charge, and the surface chemistry of nanomaterials play critical roles in the nanomaterial uptake pathways, translocation and transportation in plants. For instance, Avellan *et al.* demonstrated that the surface coating (polyvinylpyrrolidone, PVP, *versus* citrate) on gold nanoparticles (AuNPs) with diameters ranging from 3 to 50 nm plays a major role in the interaction of AuNPs with wheat leaves, their path of entry and the subsequent impact on plant health.[5] They found that the adhesion of the AuNPs to the leaf surface was increased when particle size decreased. The more hydrophobic PVP coating (compared to that of hydrophilic citrate) increased the interaction of AuNPs with the leaf surface. Using submicron resolution X-ray fluorescence (XRF) mapping, they proposed that the surface chemistry of AuNPs also affects their ability to cross the cuticle, to enter the mesophyll and to move through the plant vasculature. The study also raised questions about unintended side effects, *e.g.*

[a] *Facility for Analysis, Characterisation, Testing and Simulation (FACTS), Nanyang Technological University, 639798, Singapore. E-mail: ymlam@ntu.edu.sg*
[b] *School of Materials Science and Engineering, Nanyang Technological University, 639798, Singapore*

corona formation around the AuNPs and its influence on the fate of AuNPs in plants and the mechanism of cuticular uptake. Some of these questions can be answered by using imaging techniques with a higher resolution, for instance, scanning transmission electron microscopy (STEM). Wang *et al.* combined high-resolution secondary ion mass spectrometry (NanoSIMS) with high-angle annular dark-field scanning transmission electron microscopy (HAADF-STEM) to investigate the cellular internalization and intracellular biotransformation of silver nanoparticles (AgNPs) in unicellular green alga.[6] NanoSIMS was used to obtain the elemental distribution of Ag in the algal cells. They found that AgNPs tend to accumulate predominantly on the cell walls and in the cytoplasm of the algae. HAADF-STEM was used to examine the localization accurately and to determine if there are any changes to the morphology of the AgNPs. Although this study provides solid evidence for particle internalization and biotransformation of AgNPs, algae are typically unicellular or have simple, undifferentiated structures, which makes the uptake of nanoparticles easier to track compared to more complex, multicellular plants. As the translocation pathways can be very different for complex systems, it would be highly beneficial to have a comprehensive translocation study in multicellular plants.

In addition to stomatal entry, direct penetration of nanoparticles through the plant cuticle has been hypothesized as a possible uptake pathway,[7,8] particularly for nanoscale materials. However, most existing studies rely on indirect or surface-sensitive techniques and primarily focus on initial leaf entry, leaving the continuity of nanoparticle transport from foliar application to distal plant tissues insufficiently resolved. High-resolution, compartment-spanning visualization is therefore required to elucidate whether and how nanocarriers traverse the cuticle and subsequently translocate within multicellular plants.

As mentioned earlier, though several studies investigated the effect of nanoparticle size, shape and charge on the uptake by plants,[5,9–11] there have not been any studies on how nanocarrier morphology influences their interaction with plants after loading with agrochemicals and dyes *via* foliar application without any external force, *e.g.* infiltration *via* needle injection. A recent study compared DNA-modified Au nanospheres with different dimensions of 5, 10, 15, and 20 nm, and nanorods with a dimension of 13 × 68 nm, and found that while sub-20 nm spherical Au nanospheres associate with plant cell walls but do not enter plant cells, gold nanorods do enter cells, likely through endocytosis and a rotation-mediated process that facilitates their translocation across cell walls.[12] In that study, Au NPs were abaxially infiltrated into the leaves. The external force, such as syringe infiltration, can significantly affect the uptake and translocation of nanocarriers in plants. Additionally, their study focused solely on the distribution of nanocarriers within plant leaves, neglecting other parts such as stems and roots. This limited scope may overlook the comprehensive distribution and translocation patterns of nanocarriers throughout the entire plant. Furthermore, little information has been reported about the form of the nanoparticles once they have been taken up by plants, for example, do they remain in their original shape, dissolve as metal ions or other precipitated species of nanoparticles after uptake.[10] This is because confocal microscopy, which is commonly used to track the location of nanoparticles, is used to determine the location of the dye and the assumption is that the conjugation between the dye and the nanoparticles is maintained inside the plant. However, this might need to be re-evaluated for several reasons, such as the low dye labelling efficiency, the solubility of chromophores[13] and integrity of the nanoparticle-dye bond is challenging to maintain under harsh conditions, *e.g.* pH variation or polarity changes amongst the different tissues inside the plant. X-ray fluorescence (XRF) microscopy can be employed to provide elemental information but due to its limited spatial resolution (several tens of nm for a synchrotron X-ray source to several hundreds of nm with a normal lab X-ray source), it is not possible to determine whether the nanoparticle remains intact, or any morphology transformation happened once it is uptake by plants. Inductively coupled plasma optical emission spectrometry (ICP-OES) is an elemental technique with good sensitivity, but it again lacks spatial resolution.

In this study, we designed and synthesized monodispersed Au nanospheres and nanowires capped with hydrophilic beta-cyclodextrin (β-CD) polymer that can serve as carriers for different micronutrients. β-CD is widely used as a surface modification for biomaterials in various biomedical and pharmaceutical applications. These synthesized Au nanospheres or nanowires are loaded with micronutrients *via* physisorption while the dye molecules are adsorbed in the cavities of β-CD forming inclusion complexes. The agrochemical-loaded Au nanospheres or nanowires, referred to as Au spherical or wire nanocarriers, are subsequently applied to the eggplant leaves. Foliar application is a widely employed method in agriculture, horticulture, and gardening for various purposes. It has several advantages over soil-applied fertilizers because the nutrients are applied and taken up very quickly and directly by the stomata or epidermis, providing a specific and rapid correction of nutrient deficiency or improvement to plant health.[14,15] In this study, our aim is to understand how the shape of the nanocarrier affects their uptake by plants. Once they are successfully taken up by the plants, by following the location of these Au nanoparticles, it would be possible to elucidate the uptake pathway and understand how the various parameters affect this translocation. The structural differences between spherical and wire nanocarriers resulted in distinct uptake and distribution patterns within plant tissues and the unique geometries of these nanocarriers will lead to different interaction mechanisms with plant cell walls, which can be revealed by several complementary techniques, confocal microscopy, ICP-OES and STEM energy dispersive X-ray spectroscopy (EDX) mapping. Using HAADF-STEM and high-spatial resolution STEM-EDX we can determine the form and distribution of Au nanocarriers in the plants.

2. Experimental section

2.1. Synthesis of hydrophilic gold nanospheres and nanowires

β-CD capped Au nanospheres were synthesized by reducing gold(III) chloride ($HAuCl_4$) with β-CD polymer in alkaline aqueous solution using a method similar to that used by Aswathy *et al.*[16] Briefly, 40 mL of deionized (DI) water, 10 mL of 15 mM β-CD polymer (Product number: C2485, molecular weight: 2000–300 000 Da, Sigma-Aldrich) and 1 mL of 15 mM $HAuCl_4$ (trihydrate, ≥99.9% trace metals basis, Sigma-Aldrich) solutions were stirred at room temperature until the solution was thoroughly mixed and turned clear. Subsequently the pH of the solution was adjusted to be about 11 using NaOH solution. The solution was heated to 100 °C and maintained for 30 min while being vigorously stirred (800 rpm). The colour of the solution gradually changed from orange to pink indicating the formation of Au nanospheres. The solution was naturally cooled, then centrifuged and washed twice with DI water. The Au nanowires were prepared by the self-assembly of β-CD polymer capped Au nanospheres for an extended period, adapted from a previous report.[17] The initial reaction protocol is similar to that used for the synthesis of Au nanospheres. After heating, 0.3 mM EDTA solution was added to the mixture, which was then left undisturbed at room temperature overnight to facilitate self-assembly. The resulting nanowires were isolated and washed twice with DI water. After washing, the β-CD polymer capped Au nanospheres and nanowires were then redispersed in DI water.

2.2. Agrochemical loading

To obtain Au nanocarriers loaded with the agrochemical Cu–EDTA (ethylenediaminetetraacetic acid copper(II) disodium salt, ≥97.0%, Sigma-Aldrich) and labelled with a dye, rhodamine B (RhB), an excess of Cu–EDTA and rhodamine were sequentially added to a solution of β-CD polymer capped Au nanospheres or nanowires. RhB was used for tracking the nanoparticles in the plant using confocal microscopy. In detail, 2.25 mL of 100 mM Cu–EDTA aqueous solution was added to 10 mL of β-CD polymer capped Au nanosphere or nanowire aqueous solution, sonicated for 3 min and then transferred to a magnetic stirrer plate. After 2 h of stirring at room temperature in the dark, 1.75 mL of 24 μM of RhB (Sigma-Aldrich) aqueous solution was added and left to stir overnight. Finally, the solution was centrifuged and washed with 2–3 rounds of DI water until there was no purple colour from RhB in the supernatant. The RhB-labelled Cu–EDTA-loaded Au nanospheres or nanowires, subsequently referred to as Au spherical or wire nanocarriers, were re-dispersed in DI water or *N*-[tris(hydroxymethyl)methyl]-2-aminoethanesulfonic acid (TES) (Sigma-Aldrich) buffer (7.4 pH) for characterization or foliar application. TES buffer was selected due to its pK_a of ~7.4, which is suitable for maintaining physiological pH, its low propensity for metal ion complexation, and its established use as a plant-compatible buffer in similar nanoparticle delivery studies.[18,19]

2.3. Plant growth and Au nanocarrier application

Solanum melongena (eggplant) was chosen as the plant for the experiment. Our plants were grown in a CMP6010 growth chamber (Conviron) with 200 μmol s^{-1} m^{-2} air ventilation, 60% relative humidity, a day and night temperature of 22 °C and 18 °C respectively and a light–dark cycle of 16 h:8 h. Soil (Organic Vegimix soil from Baba ™ Kean Beng Lee Industries SDN BHD) was mixed with vermiculite in a ratio of 2:1. Seeds (Hort Garden Pte Ltd) were placed on water-moistened towel paper in a zip-block bag and kept in the dark at room temperature for germination. After sprouting, 2 seedlings were transferred to each ~15 cm diameter pot and then grown in a growth chamber. Plants were watered as needed with untreated water. Once the plants had sprouted at least 4 true leaves, two concentrations of nanocarrier were applied and subsequently referred to as the low concentration and high concentration. For the low concentration treatment groups, spherical (9.28 μg mL^{-1} elemental Au) or wire (9.54 μg mL^{-1} elemental Au) nanocarriers were prepared in TES solution. This solution was gently applied manually using a flat art brush to both adaxis (predominantly) and abaxis surfaces of two fully expanded leaves per plant with 10 mL applied per leaf during each round. The treatment consisted of three applications performed on day 0, day 1 and day 2. During foliar application, any excess runoff was promptly wiped away with a tissue. The high concentration treatments were attained by doubling the volume of the Au stock solution while maintaining a consistent total application volume. Some plants were treated as controls and had no nanocarrier applied. The plants were harvested on day 3.

2.4. Plant sample fixation and embedding

Fresh leaves, stems or roots from the eggplants treated with the medium concentration were harvested after 3 days and flushed with DI water with gentle brushing to remove particle agglomeration from the surface, followed by washing with ethanol. Samples were cut into areas ~1–2 mm^2 and initially fixed in 2.5% glutaraldehyde (v/v) in pH 7.4 phosphate buffer solution. On the following day, the primary fixative was removed and the samples were washed 3 times with phosphate buffer saline (pH 7.4). Samples were immersed in secondary fixative (1% uranyl acetate solution). After 2 h in a rotary mixer at 80 rpm (Pelco R2), the secondary fixative was removed and samples were washed 3 times with DI water. The samples were dehydrated by immersion in a series of ethanol solutions with increasing concentrations followed by 3 rinses in pure acetone, each time for 20–30 min at room temperature. Subsequently, the samples were immersed in different ratios (1:2, 1:1, 2:1 and 3:1) of LR White (LR White medium grade, EMS)-acetone mixture for 1 h for 1–2 times at room temperature, then pure LR White at 4 °C overnight. The fixed specimens after recovery at room temperature were transferred into gelatine capsules, positioned at the tip of the capsules, sealed, and cured at 60 °C for 2–3 days.

2.5. Characterization

For size, morphological and elemental composition information, nanospheres, nanowires, and their respective nanocarriers were dispersed in DI water. The nanocarrier solution was dropcast on carbon-coated nickel or molybdenum grids. For tracking the location of the nanocarrier in the plant, the pyramidal ends of the plastic blocks were trimmed, sliced with an ultramicrotome (UC7, Leica microsystems) and put on 200 mesh carbon-coated Ni grids (Ted Pella). HAADF-STEM images, TEM images, and EDX maps of Au nanocarriers were collected using an aberration-corrected JEOL JEM-ARM200F TEM operated at 200 keV with an Oxford X-Max TLE 100 mm^2 windowless silicon drift detector (SDD) EDX, an aberration-corrected JEM-ARM300F TEM operated at 300 keV with a JEOL JED-2300T 100 mm^2 windowless SDD detector EDX, and a JEOL 2100F TEM operated at 200 keV with a 100 mm^2 windowless Oxford Ultim Max detector EDX. The zeta potential (ζ) was used to measure the electrostatic interaction between the surface of the Au nanospheres, nanowires and their respective nanocarriers and the liquid medium. The zeta potential of aqueous suspensions of above-mentioned nanomaterials in 10 mM TES buffer solution (pH 7.4) was measured using a Nano Particle Analyzer SZ-100 (HORIBA). The optical absorption of RhB, Cu–EDTA, Au nanospheres, Au nanowires, and their respective nanocarriers in aqueous solution was tested using a UV-visible spectrophotometer (UV-2700, Shimadzu). Fourier-transform infrared spectroscopy (FT-IR, Perkin Elmer Frontier) was used to identify the surface functional groups of the AuNPs, agrochemical and dye adsorption. Au nanospheres, nanowires, and their respective nanocarriers dried at 60 °C were mixed with KBr before being compressed into a pellet. The spectra were recorded from 400 to 4000 cm^{-1} over 64 repetitions.

To monitor the uptake and translocation of the nanocarriers in the plants using confocal fluorescence microscopy, fresh plant leaves, stems and roots were harvested from the plants. Au nanocarriers on the surface of the leaves were brushed away then samples were washed with DI water, cut and mounted on a glass slide. DI water was added to prevent cell dehydration. Samples were imaged using a laser scanning confocal microscope (LSCM, Leica TCS SP5). A laser excitation of 543 nm was used to locate the dye in the plant samples and 633 nm excitation was used for chlorophyll. The photomultiplier tube (PMT) detection range was set to 550–620 nm for RhB and 650–750 nm for chloroplast autofluorescence from chlorophyll.

The Au and Cu concentrations in dried plant samples and the stock solutions were measured using ICP-OES. Leaf, stem and root samples from the plants were collected, washed with deionized water, and then oven dried at 75 °C for ~2 days. Dried plant samples were ground, weighed and microwave-assisted acid digested to extract elements. Microwave digestion was carried out using an UltraWAVE™ microwave oven (Milestone Microwave Laboratory Systems, Germany) at 230 °C for 10 minutes with concentrated nitric acid (HNO_3, Sigma-Aldrich). The concentrations of Au and Cu were determined using an Optima 8300 ICP-OES (Perkin Elmer, USA). Commercial standard solutions (PerkinElmer) of copper and gold were used for calibration. The calibration curves obtained for all the studies had correlation coefficients of at least 0.99. The nutrient loading rate of Cu–EDTA on Au nanocarrier was calculated by dividing the detected concentration of Cu in the stock solution by the sum of the Cu and Au concentrations.

3. Results and discussion

3.1. Design of the Au nanocarrier

Cyclodextrins (CD) are cyclic oligosaccharides containing D-glucose units connected *via* α (1,4) glycosidic bonds. Common cyclodextrins contain six, seven or eight D-glucose units. They have been widely used as an ideal functional molecular host to modify the surface of nanoparticles.[20–23] β-CD polymer has been used for the development and construction of biomaterials such as hydrogels, nanoassemblies and nanocarriers.[24,25] The host–guest interactions between β-CDs and guest molecules are mainly driven by the hydrophobic associations.[23] The toroidal cavity of β-CDs has a hydrophobic interior and a hydrophilic exterior. The stability of the inclusion complex formed between β-CD and the guest molecule also determines the release behaviour of the guest molecule. It was thought that CD can act both as a reductant and as a capping agent in Au and cadmium telluride nanoparticle synthesis.[26,27]

Scheme 1 shows a schematic drawing of the stepwise preparation of the Au spherical and wire nanocarriers used in this study. β-CD polymer capped-Au nanospheres or nanowires were synthesized, loaded with the agrochemical followed by the dye. Copper (Cu) is one of the micronutrients necessary for plant growth and acts as a structural component of proteins and enzymes. It also participates in the various vital growth processes such as mineral nutrition, photosynthesis, mitochondrial respiration, cell wall metabolism and hormone-signalling pathways.[28] It is essential for the building and the conversion of amino acids to proteins. EDTA has four carboxylic groups, which are dissociated to give a tetravalent anion, thus the Cu–EDTA complex has a net charge of −2 and a very stable chelate can be formed between one molecule of EDTA and Cu^{2+}.[29]

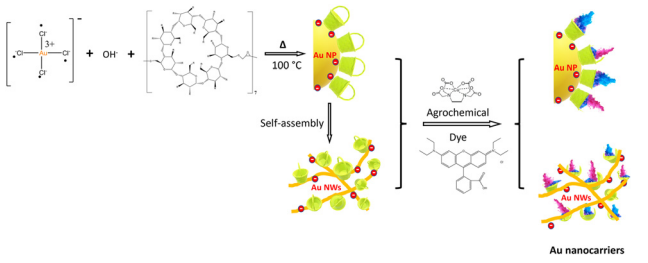

Scheme 1 Schematic drawing showing the preparation of nanospheres, nanowires, and their respective nanocarriers.

Due to the presence of these carboxylic groups, Cu–EDTA exhibits hydrophilic properties. In this study, given its hydrophilic nature, Cu–EDTA is unlikely to be encapsulated inside the hydrophobic cavity of β-CD; instead, it more plausibly interacts with the hydroxyl groups on the exterior surface of β-CD through hydrogen bonding and electrostatic interactions when coating the Au nanoparticles. Cu–EDTA has been widely used to increase the availability of Cu to plants or Cu management in agriculture.[30] RhB is widely used as a tracer dye in biology or biotechnology applications, such as in fluorescence microscopy to determine the rate and direction of flow and transport.[21,22,31] RhB is reported to enter the β-CD's cavity *via* a hydrophobic interaction.[21] RhB is used to track the location of the Au nanocarriers using confocal microscopy. AuNPs are attractive as nanocarriers because of their inertness, biocompatibility, and high contrast in TEM.[32–34] In plants, Au nanospheres and nanowires have been used to track morphology and location. Beyond imaging, their use as carriers offers opportunities for targeted delivery and controlled release of agrochemicals, potentially more effective than foliar Cu–EDTA solution alone.

Physical characterization. The size, morphology and composition of our Au nanospheres, nanowires, and their respective nanocarriers were studied using TEM and STEM-EDX (see Fig. 1 and S1 and S2 for additional images and EDX results, SI). TEM analysis revealed that both the spherical and wire nanocarriers have narrow size dispersity and crystallinity. The size and morphology of the nanospheres or nanowires remained constant even after loading them with agrochemicals. As shown in Fig. 1A, as well as Fig. S1 SI, the average diameter of the Au nanospheres was 8.8 ± 1.0 nm. The Au nanospheres exhibited lattice spacings of ~2.4 Å corresponding to the (111) planes of face-centered cubic (FCC)-gold.[35] Details regarding the size, morphology, and crystallinity of Au wire nanocarriers can be obtained from the HAADF-STEM image shown in Fig. 1B and S2, SI. The average diameter of the Au nanowire is found to be 9.6 ± 3.1 nm, while the length ranged from a few tens of nanometres to several micrometres. Due to significant entanglement and agglomeration of the nanowires, a statistically meaningful average length could not be reliably determined. The increase in the diameter of the nanowires compared to the spherical nanoparticles was attributed to the self-assembly process or the Ostwald ripening effect at a lower concentration of the capping agent, β-CD polymer, as reported previously.[17]

As mentioned previously, the nanowires were formed *via* self-assembly of nanospheres followed by transformation into nanowires. The following mechanism is proposed: due to the use of a relatively low molar ratio of β-CD polymer to Au precursor, β-CD polymer may only partially cover the surface of the Au nanospheres, resulting in a thermodynamically unstable system.[36] The hydrophobic portions of the β-CD polymer-capped Au nanospheres interact with the hydrophobic cavity of the β-CD units in the polymer. Instead of wrapping around the surface of the nanospheres, the β-CD polymer guides the oriented

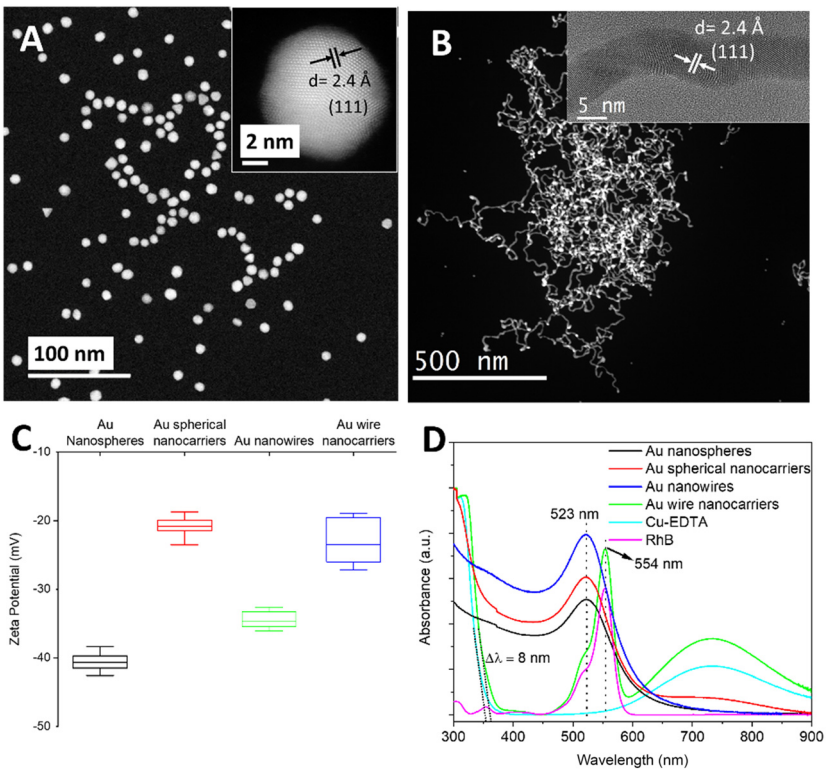

Fig. 1 HAADF-STEM images of (A) spherical and (B) wire-shaped Au nanocarriers. Inset: High resolution STEM image showing the Au lattice spacings. (C) Box plot of the zeta potential of the Au nanospheres, nanowires and their respective nanocarriers. (D) UV-vis absorption spectra of Au nanospheres, nanowires, and their respective nanocarriers after Cu–EDTA and RhB loading, compared with those from Cu–EDTA and RhB.

attachment of nanospheres along its chain, resulting in elongated complexes such nanowires. The β-CD polymers facilitate the oriented attachment of the nanospheres, promoting the formation of elongated structures, *e.g.* nanowires.[17] Fig. S1B–F and S2B–F show STEM-EDX elemental maps of the Au spherical and wire nanocarriers. They reveal that after sequentially adding Cu–EDTA and RhB to the nanocarriers, the Cu signal from Cu–EDTA and the Cl signal from RhB can be detected from the Au nanocarriers but not from the residue of the gold precursor (see Fig. S3 for EDX linescan profile, SI), indicating the successful adsorption of agrochemical Cu–EDTA and dye RhB on both Au nanospheres and nanowires *via* physisorption. Based on ICP-OES tests of Au spherical and wire nanocarrier solutions, the Cu–EDTA loading rates are calculated to be 35.7 and 64.5% by mass of Cu to Au, implying a high loading capacity for nanowires due to their anisotropic shape and thus a large surface area to volume ratio of nanowires.[36]

Surface charge. As mentioned previously, the surface charge can affect the uptake of the nanoparticles. The interaction of the β-CD polymer molecules with AuNPs was reported to occur through conjugation between the carboxyl groups, which are oxidized from the reacted hydroxyl groups of the β-CD polymer and the Au surface *via* a O–Au bond.[23] This conjugation can effectively stabilize the AuNPs. The electron transfers from the O atoms of the carboxyl groups of β-CD polymer to the surface of the AuNP and can result in a negatively charged AuNP surface.[37] The zeta potential measurements were used to determine the surface charge of these nanospheres, nanowires, and their respective nanocarriers in a TES buffer solution (pH 7.4). The preloaded Au nanospheres and nanowires (without the agrochemicals) have negative zeta potentials of −40.08 ± 1.62 mV and −34.42 ± 1.45 mV, respectively (see Fig. 1C).

Previous studies of nanoparticle uptake in plants have found that nanoparticles with sufficiently high positive or negative surface charge (typically $|\zeta| > 20$ mV) can enhance interactions with plant cell walls or chloroplast membranes.[10] In the present study, the Au nanocarriers exhibit moderate negative zeta potentials after agrochemical loading (−21.17 ± 1.77 mV for nanospheres and −23.1 ± 3.58 for nanowires; see Fig. 1C). These values indicate a modest surface charge that may influence nanoparticle–leaf surface interactions during foliar application but do not imply high electrostatic stability in colloidal terms.

Nanoparticle uptake in plants is governed by multiple factors, including morphology, size, surface chemistry, and the physicochemical environment at the leaf interface, rather than zeta potential alone. The β-CD capping layer is expected to interact weakly with the Au surface and may be sensitive to changes in ionic strength and pH. Upon agrochemical loading, Cu–EDTA is more likely to associate with the β-CD layer through weak interactions such as hydrogen bonding and electrostatic effects, rather than displacing β-CD from the Au surface. Consistent with a report that ligand adsorption can modulate nanoparticle surface charge,[38] the observed decrease in zeta potential ($\Delta\zeta$ = 18.91 mV) after Cu–EDTA and RhB loading reflects changes in the surface chemistry of both spherical and wire nanocarriers.

Agrochemical loading capacity. The optical absorption peaks of the as-synthesized β-CD capped Au nanospheres and nanowires can provide some hints to the agrochemical loading capacity. Both nanostructures appear to have a strong transverse plasmonic resonance at around 523 nm (see Fig. 1D). The longitudinal surface plasma peak, which typically appears above 600 nm in Au nanowires, is absent probably due to the rough morphology. There is a small hump between 332 nm and 387 nm in the absorption spectrum of Au nanowires, which probably relates to the high aspect ratio of the nanowires. In the absorption spectrum of Au spherical nanocarriers, the strong plasmonic resonance peak almost stays at the same wavelength after Cu–EDTA and RhB loading. The sharp peak at 554 nm from RhB is missing, instead a weak shoulder between 500 nm and 523 nm is visible, which is from RhB. A broad hump between 620 nm and 880 nm in the Au spherical nanocarriers is from Cu–EDTA. In the absorption spectrum from the Au wire nanocarriers, the strong absorption maximum at around 554 nm from RhB and the broad absorption hump between 590 nm and 600 nm from Cu–EDTA are prominent. The strong transverse plasmonic resonance peak at 520 nm from the nanowires has changed to a shoulder. The early rise in absorption of 8 nm may arise from the hump (332–387 nm) observed for Au nanowires. It is observed that in the Au wire nanocarrier absorption spectrum, peaks from RhB and Cu–EDTA are much stronger than those from spherical nanocarriers, implying the nanowires have a higher agrochemical loading capacity.

Chemical bond formation. FT-IR spectroscopy is a quantitative analytical technique used to identify the bonding mechanisms in bulk and on surfaces.[39,40] FT-IR was used here to confirm the presence of the macrocyclic structure of β-CD on the surface of the Au nanospheres and nanowires, as well as the inclusion of Cu–EDTA and RhB. After agrochemical and dye loading, it is found that some of the FT- IR bands are still maintained while some of them showed significant band shifts. FT-IR spectra of the gold nanospheres, nanowires and their respective nanocarriers, along with spectra from β-CD polymer, Cu–EDTA, and RhB, are presented in Fig. 2. Colour bars (I–VI) are used to illustrate the primary changes in the spectra. A summary of main IR frequencies with assignments is presented in Table S1, SI.

The vibration in the range of 3675–3165 cm^{-1} as indicated by colour bar I (Fig. 2), is typically associated with stretching vibrations of hydrogen-bonded O–H (hydroxyl) groups, *e.g.* from the carboxylic groups or adsorbed water molecules. The strong vibration bands at 3543 and 3329 cm^{-1} from the Au nanospheres was assigned to multiple O–H stretching.[41] It was reported that the hydroxyl groups of β-CD molecules participate in the reduction of Au^{3+} ions to metallic Au^0.[23] Based on the analysis of XPS results, the authors proposed that the hydroxyl groups of the β-CD molecules are oxidized to carboxyl groups.[23] A prominent band at 3425 cm^{-1} observed in the nanowires, spherical and wire nanocarriers as well as in Cu–EDTA is assigned to OH groups from β-CD polymer and EDTA, and physically absorbed water molecules.

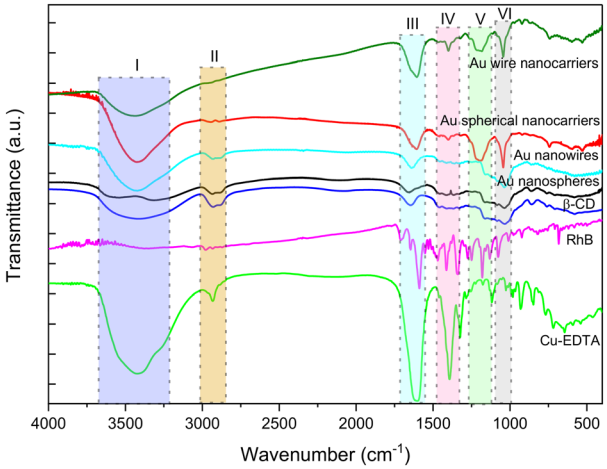

Fig. 2 FT-IR spectra from Au nanospheres, nanowires and their respective nanocarriers compared with spectra from Cu–EDTA, RhB, and β-CD polymer. Colour bars (I–VI) highlight key spectral changes.

As indicated by colour bar II (Fig. 2), the vibration in the range of 3003–2845 cm^{-1} shows a characteristic frequency at 2942 cm^{-1} and 2949 cm^{-1} in the nanosphere and wire nanocarriers, corresponding to the C–H band in chelated molecules.[42] This implies that the COO^- groups of EDTA are still attached to the Cu ions in both shaped nanocarriers. The bands observed at 2938 cm^{-1} can be assigned to CH_2 bending,[43] while the band at 2885 cm^{-1} corresponds to aliphatic C–H stretching. Within the vibration region marked by bar III, several bands located at 1705, 1663, 1604 and 1592 cm^{-1} are identified. These bands are assigned to carbonyl stretch, ν(C═O) of the ester group from RhB, H–O–H deformation bands of adsorbed water molecules, the asymmetric stretch, ν_a(C═O) of the COO^- group of Cu–EDTA and/or β-CD polymer, and in-plane C═C skeletal stretching vibration. In the nanosphere spectrum, a weak band at around 1604 cm^{-1} is probably due to the oxidation of cyclodextrins by tetrachloroaurate and the interaction with the AuNP surface *via* the O–Au bond which effectively stabilises the Au nanospheres.[27] In the spectra from the spherical and wire nanocarriers, the very strong vibration bands ν(C═O) at 1606 and 1601 cm^{-1}, reflecting the covalent character for the Cu–carboxylate bond,[42] overlap with those of β-CD polymer capped Au nanospheres and nanowires. Similarly, within the vibration region of 1439–1291 cm^{-1} (colour bar IV, Fig. 2), stretching bands of –COO from Cu–EDTA and RhB are present in the nanospheres, nanowires and their respective nanocarriers. For example, the band at 1414 cm^{-1} due to the characteristic vibration of the carboxyl group present on the Au spherical nanoparticle surface.[16] A characteristic band at 1391 cm^{-1} due to the C═O group shifts to higher frequencies (1398 and 1402 cm^{-1}) and the intensities decrease, which might be attributed to an increase in the strength of the N–Cu bond.[42] Another band at 1326 cm^{-1} assigned to the COO^- group shifts to 1320 cm^{-1} due to the filling of the $d_{subshell}$.

After agrochemical loading, a noticeable difference between nanospheres/nanowires and nanocarriers becomes evident at colour bar V (Fig. 2). For example, strong vibrations from the O–H bending and C–N stretching between 1225–1180 cm^{-1} are absent in the spectra of ß-CD polymer and Cu–EDTA. These vibrations could be assigned to a C–O characteristic peak from an ester bond, indicating the interaction of the carboxylic acid of Cu–EDTA with hydroxyl groups of β-CD. This suggests the successful loading of RhB in the nanocarriers.[44] In the vibration region of 1078–975 cm^{-1} as shown in colour bar VI, the strong band at around 1037 cm^{-1} is assigned to the coupled stretch vibration ν(C–C/C–O). In addition, the band at 1161 cm^{-1} which corresponds to the asymmetric glycosidic vibration ν_a(C–O–C) and the band at 1084 and 1037 cm^{-1} corresponding to the coupled stretch vibration ν(C–C/C–O) are clearly observed and the characteristic bands of polysaccharide, indicate that Au nanospheres have been successfully encapsulated by polysaccharide.[22,45] The band at 861 cm^{-1} corresponding to the out-of-plane bending vibration γ(C–H) of the β-CD polymer appears in nanosphere, nanowires and their respective nanocarriers. Cyclodextrin cavities are expected to capture RhB molecules through the formation of inclusion complexes.[21,44] These bands appear in both nanocarrier spectra, suggesting that Cu(II) ions might not inhibit RhB adsorption onto β-CD polymer-capped Au nanocarriers. The inner diameter of the β-CD cavity is about 0.78 nm, which allows the arms of the RhB molecule, with a diameter of around 0.31 nm, to insert into the β-CD cavities *via* hydrophobic interactions while the remaining parts extend outward, providing sites for metal binding.[21,44] This implies that the interaction between RhB and the β-CD polymer-capped nanocarriers is strong enough to remain unaffected by the presence of Cu(II) ions in the system, due to specific molecular interactions within the system. The adsorption of dye by CD cavities on Au nanocarriers could create new specific adsorption sites for other agrochemicals containing metal ions. Based on the above results, the FT-IR spectra confirmed that β-CD polymer is effectively bound to the surface of the Au nanospheres and nanowires, and an agrochemical and dye are successfully loaded onto the surface of Au nanoparticles.

3.2. Translocation study

3.2.1 Optical studies using confocal fluorescence microscopy. Next, we would like to understand how these specially designed and synthesized nanocarriers were taken up by eggplants. Nanocarriers were introduced *via* foliar application without any external force such as infiltration, which would have disadvantages for example a non-uniform distribution of nanoparticles, injury to plant tissue, risk of infection, stress induction, and limited uptake mechanisms. The fluorescence signals from RhB (in red), partially located inside the cavities of β-CD on Au nanocarriers, and from autofluorescent compounds (in blue), such as chlorophyll where present and were monitored in the leaves, stems, and roots (see Fig. 3). The bright red regions in the image indicate the locations where the agrochemical is delivered and potentially released to the plant. Confocal fluorescence

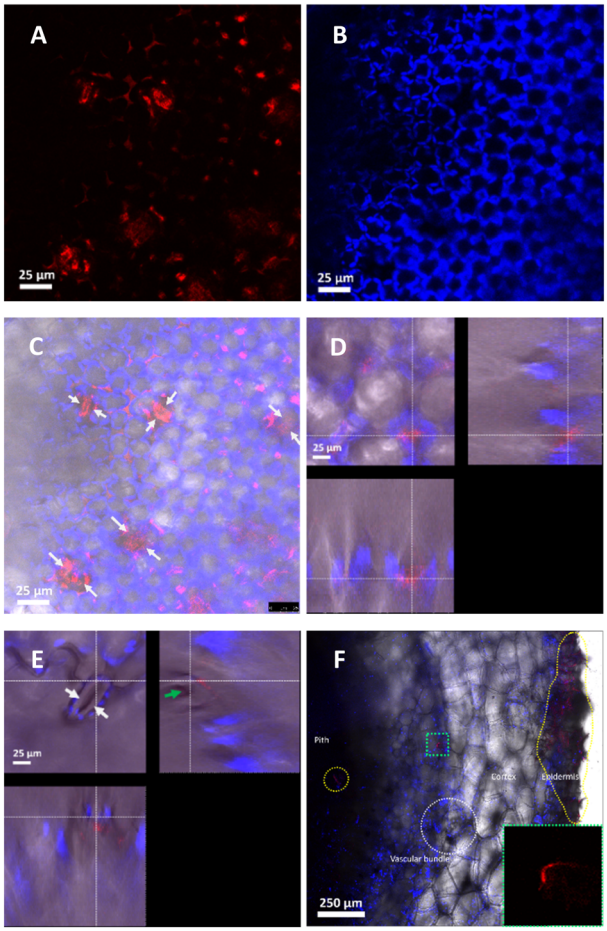

Fig. 3 Confocal fluorescence microscope images showing the biodistribution of RhB-labelled spherical nanocarriers in eggplant (A–E) leaves and (F) stem. (A) RhB signal (in red), (B) autofluorescence signal from chlorophyll (in blue), and (C) signals overlapped on a brightfield image obtained from the same region of the leaf. Orthogonal views of representative confocal microscopy z-stacks displaying the colocalization of Au nanocarriers in (D) extracellular space of mesophyll cells, (E) stomatal guard cells (white arrow) and stomatal pore (green arrow). *Z*-Stack scan from leaf sample: *Z*-stacks (1.0 μm *z*-axis resolution, total 63.4 μm scanned, 63 × 63 nm voxel *x*–*y* resolution). Note: The inset in image (F) corresponds to the area marked by the green dotted box on the stem. The dotted yellow regions indicate the presence of nanocarriers.

microscopy images of leaves indicate that the Au nanocarriers have successfully penetrated through the leaf surface (see Fig. 3A–E). However, we are not able to confirm whether after foliar application the Au nanocarriers are taken up *via* the cuticle or stomata using confocal microscopy due to its low resolution.[14] Previous studies showed that stomata are protected against infiltration of aqueous solutions because of their geometry and the hydrophobic pore walls.[46,47] In our case, similar constraints may prevent the uptake of our hydrophilic nanocarriers *via* stomata. The spatial distribution of the Au nanocarriers within the plant leaf can be seen from the high resolution image and the orthogonal views, which are reconstructed from multiple *Z*-stack images, collected with a *Z* step size of 1 μm per scanning layer, which is smaller than the chloroplast size (5–10 μm) (see Fig. 3D and E).[18] Fig. 3D shows the presence of the fluorescence signal from the Au nanocarriers in the extracellular space and the mesophyll cells.

The process of foliar applied nutrient uptake by plants through the cuticle pathway is proposed to have three stages.[48] Firstly, the applied substances penetrate the cuticle and the cellulose-rich cell wall *via* limited or free diffusion (no additional energy required). Then they are adsorbed onto the surface of the plasma membrane *via* a binding process or selective permeability including passive and active transports. Finally, they are taken up into the cytoplasm. This process requires metabolically derived energy.[48] We repeatedly observed the presence of the RhB signal in the regions which contain no stomata and are close to the epidermis in the *Z*-stack scans. Fig. 3E shows the presence of RhB fluorescence signals from the Au nanocarriers in stomatal guard cells or pores, implying the involvement of multiple pathways in the uptake of nanocarriers. Confocal fluorescence imaging also reveals vein-associated signal distributions after foliar application (see Fig. S4, SI), which may indicate potential transport pathways. Given the possibility of dye leaching, these observations are considered supportive and are primarily used to guide interpretation of the TEM results. For these nanocarriers, short-distance transport involving the transport of substances from cell to cell, *via* apoplast pathway or symplast pathway, within tissues or organs essentially plays an important role in controlling the movement of carried nutrients, while long-distance transport of sap, *e.g.* from leaf to stem then to root, within the xylem and phloem works at the level of the whole plant.[14,49,50] Water and solutes, *e.g.* mineral salts, travel through the xylem while sucrose and amino acids are transported between the leaves and other parts of the plant by the phloem. The selective permeability of the plasma membrane controls the movement of solutes between the cell and the extracellular solutions.[49] So in our case, after the uptake of nanocarriers, phloem may transport them from the leaf, *via* veins, petiole, to the stem and finally to the roots. The translocation process is affected by the surface engineering and morphology of the nanocarriers. Cyclodextrin has excellent biocompatibility and unique inclusion capability which make it especially attractive for engineering novel functional materials for drug or nutrient delivery.[51]

RhB fluorescence is also observed in stem phloem regions and the roots (see Fig. 3F, S5 and S6, SI), suggesting that nanocarriers could travel from the foliage to the stem and then to the roots after foliar application. It is worth mentioning that the presence of RhB signals in the epidermis (outer dotted circle regions), the vascular bundle containing the phloem, and the cambium and the pith in Fig. 3F and S5, SI indicates that the nanocarriers are well distributed after translocation and/or translocated *via* different paths. As these Au nanocarriers have RhB bound to their surface, one can follow the distribution by observing the fluorescence signal from RhB. It is found that the signal is lower in the roots than in the stem, we can thus conclude that there are fewer nanocarriers translocated to the root given that the

nanocarriers and dye are still bound together with nanocarriers. Although confocal microscopy demonstrates that nanocarriers are taken up and translocated inside the plant, they are mainly found to accumulate in the plant leaves and stem, and this was further confirmed by ICP-OES and STEM-EDX which will be discussed next.

3.2.2 Chemical studies using ICP-OES. The presence of nanocarrier elements, Au and Cu, in different parts of the eggplants was confirmed by ICP-OES measurements (see Fig. 4). To study the effect of the Au nanocarrier morphology and nominal exposure level on plant uptake and internal distribution, spherical and wire-shaped Au nanocarriers were applied to leaves at two concentrations (subsequently referred to as "low concentration" and "high concentration"). The high concentration represents to a twofold increase over the operational low concentration and was employed to verify whether morphology-dependent uptake trends persist at elevated exposure. These concentrations were chosen to enable a controlled mechanistic comparison of nanocarrier morphology rather than to represent environmentally or agriculturally relevant exposure levels.

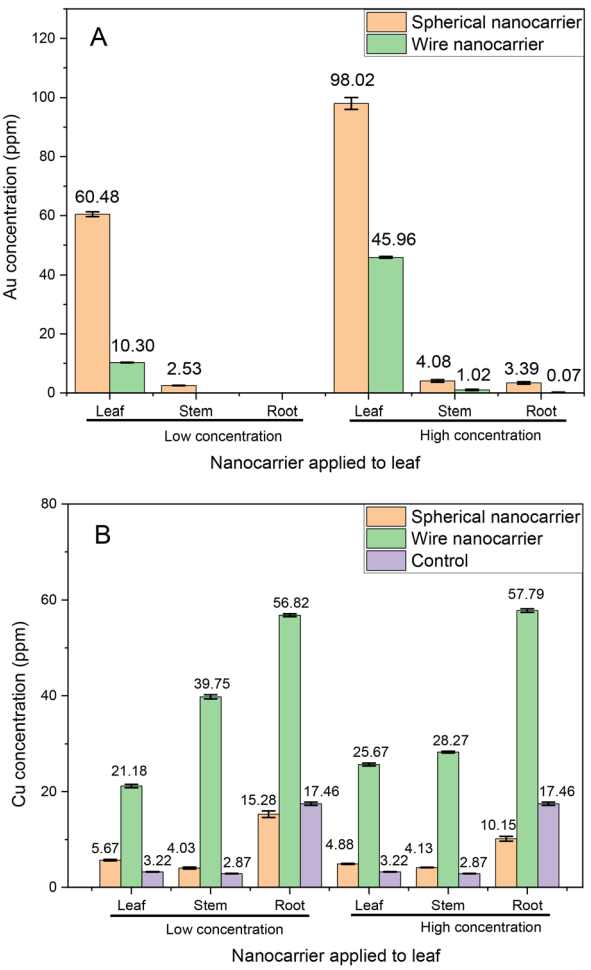

Fig. 4 ICP-OES results from eggplant tissues after foliar application of spherical and wire-shaped Au nanocarriers at low and high nominal concentrations for 3 days. (A) Au concentrations and (B) Cu concentrations measured in leaves, stems, and roots. Au concentrations below the instrumental limit of detection are not shown. Error bars represent instrumental repeatability (n = 3) of ICP-OES measurements performed on the same digested sample and do not reflect biological variability.

Although almost identical suspension concentrations and application protocols were used for spherical and nanowire nanocarriers, the exact mass of material retained on the leaf surface was not directly quantified. Losses during foliar application (*e.g.*, runoff and incomplete adhesion), post-harvest washing, and uncertainties associated with drying and grinding of plant tissues introduce unavoidable variability. Consequently, the ICP-OES results should be interpreted as semi-quantitative indicators of relative accumulation and distribution, rather than as absolute uptake values. Statistical comparisons between treatments were not performed due to the absence of biological replication.

As shown in Fig. 4A, Au was predominantly detected in leaves, followed by stems and roots, indicating limited downward translocation after foliar application. When comparing nanocarrier morphology, higher Au concentrations were consistently observed in plants treated with spherical nanocarriers relative to nanowires at both nominal exposure levels. This trend suggests that nanocarrier morphology influences foliar retention and/or subsequent uptake and internal transport. The enhanced accumulation associated with spherical nanocarriers may be related to their isotropic geometry, which can facilitate interaction with leaf surfaces and cellular barriers, whereas the high aspect ratio of nanowires may hinder internalization and promote aggregation, reducing their effective bioavailability. While increasing the nominal exposure level led to higher detected Au concentrations for both morphologies, the relative difference between spheres and wires remained evident.

Fig. 4B presents the Cu concentrations measured in leaf, stem, and root tissues. Cu originates from both Cu–EDTA associated with the Au nanocarriers and endogenous uptake from soil, as confirmed by control samples. Across all treatments, Cu accumulation was highest in the roots, consistent with the dominant role of roots in Cu uptake and sequestration. For control plants and those treated with spherical nanocarriers, the Cu distribution generally followed the order root > leaf > stem, whereas for nanowire-treated plants the order root > stem > leaf was observed. Notably, Cu concentrations in plants treated with nanowire nanocarriers were substantially higher than those measured for spherical nanocarriers and controls across all plant compartments.

As mentioned earlier, such nanocarrier systems may offer opportunities for targeted delivery and controlled release of agrochemicals, rather than permanent immobilization of the active species.

The disproportionate increase in Cu relative to Au, particularly for the nanowire treatments, indicates that Cu and Au do not remain fully coupled during or after foliar application. The Cu : Au ratio is therefore not conserved between the initial nanocarrier suspension and the harvested plant tissues, reflecting partial decoupling of Cu from the Au nanocarrier.

This behaviour is consistent with partial dissociation or leaching of surface-associated Cu species, arising from the weaker coordination of RhB/Cu–EDTA compared with the interaction between the Au nanocarrier and its stabilizing ligands. As discussed earlier, such behaviour may facilitate nanocarrier systems designed for targeted delivery and controlled release, rather than permanent immobilization of the active species.

Overall, the ICP-OES results highlight a morphology-dependent influence on the relative accumulation and distribution of Au and Cu, while also underscoring the complex and partially decoupled behaviour of metal species in planta. These findings should be interpreted qualitatively, given the uncertainties associated with foliar dose retention and the lack of biological replication.

3.2.3 Nanoscale observation using STEM. To investigate whether Au spherical and wire nanocarriers undergo any transformation during the uptake and translocation process, HAADF-STEM and high-spatial resolution STEM-EDX were employed. These advanced techniques allow for precise determination of the distribution of nanoparticle and elemental composition within various materials.[52] HAADF imaging in STEM mode is highly sensitive to the atomic number (Z) of the atoms, with the image intensity approximately proportion to Z.[2] Objects with higher atomic numbers appear bright (white) in contrast, while those composed of lighter elements exhibit darker contrast.

Fig. 5 illustrates the presence of spherical and wire-shaped nanocarriers as white dots or line segments in the cross-sectioned eggplant leaf samples. Regardless of their initial morphology, Au nanocarriers were predominantly localized along the cuticle layer following foliar application. A typical plant leaf structure comprises several distinct layers: the cuticle, epidermis, palisade mesophyll, and spongy mesophyll. The ultrastructure of the cuticle is clearly visible by the contrast differences observed under TEM.[53] The cuticle, the outermost protective layer of leaves, fruits, flowers, and non-woody stems, provides vital mechanical support and defence against drought, extreme temperatures, UV radiation, mechanical damage, and pathogens.[54] The cuticle in eggplant leaves typically measures 1–4 μm in thickness,[55] covering the epidermis and forming the outer surface layer. In Fig. 5A–C, the green dashed line represents the cuticle. Spherical nanocarriers are clearly visible, maintaining their original size and shape as shown in Fig. 5C. It seems that nanocarriers adhere to and translocate along the cuticle without penetrating the epidermis or the mesophyll cell. At higher magnification, Fig. 5B reveals a detailed view of the spherical nanoparticles embedded within the cuticle, consistent with observations reported by Kohay *et al.*[7] In that study, layered double hydroxide (LDH) nanocarrier applied on the adaxial leaf surface were found to embed within the cuticle and accumulate at anticlinal pegs between epidermal cells, with uptake pathways strongly dependent on leaf surface—predominantly cuticular penetration on the adaxial side and stomatal entry on the abaxial side. However, direct and high-resolution evidence for nanocarrier localization at the subcellular level remains scarce due to the limitations of the confocal microscopy techniques employed in that study, and no TEM studies were conducted,

The area highlighted by the white dashed square is further magnified in Fig. 5C, where the white dots represent the Au spherical nanocarriers. Interestingly, these spherical nanocarriers do not agglomerate or form clusters within the cuticle. Nanocarriers can adhere to or interact with the cuticular waxes before being taken up into the plant through stomata, trichomes, or other openings.

Fig. 5D–F show a heterogeneous population of Au nanostructures in cross-sectioned leaf samples, comprising small nanoparticles, short rods, and truncated wire-like segments.

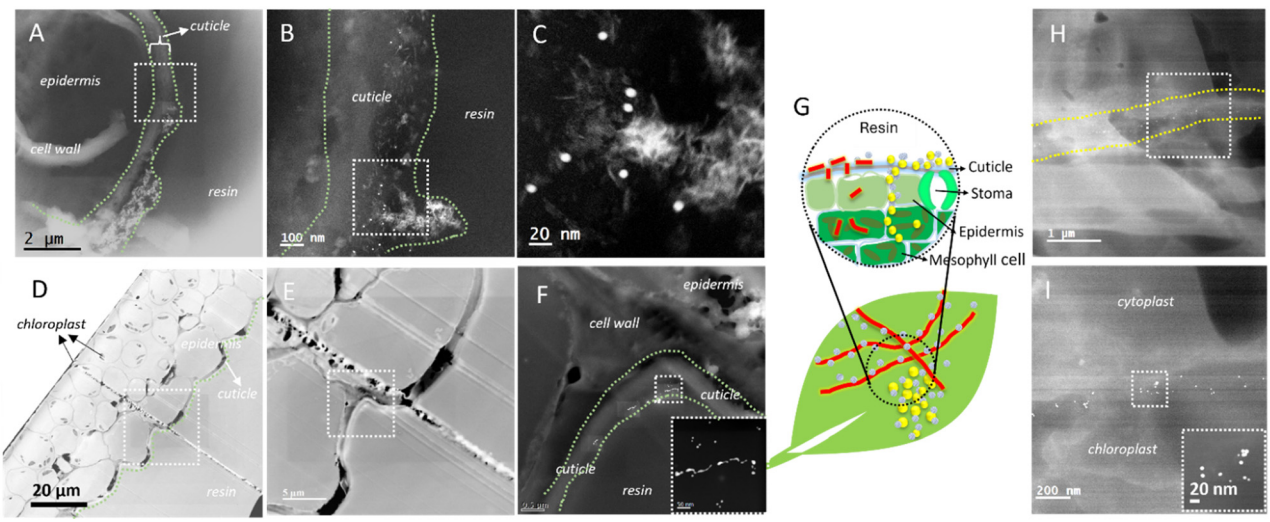

Fig. 5 HAADF-STEM images of (A–C) Au spherical and (D–F, H and I) wire nanocarriers in eggplant leaves and (G) a schematic drawing showing uptake and translocation of nanocarriers. Green dotted lines indicate the cuticle; yellow dotted regions highlight areas containing nanocarriers; white dotted boxes mark the regions of interest.

We acknowledge that smaller nanostructures are present in the initial suspension (Fig. 1B and S2A and B); however, this fraction represents a minor component of the total nanocarriers (estimated to be <10%), with the suspension being dominated by long, continuous nanowires.

A close-up view in Fig. 5F and its inset shows that the short rods and nanoparticles within the cuticle are frequently observed in close proximity, aligned along a common direction and forming chain- or "pearl-necklace"-like assemblies. Such clustered and anisotropic arrangements are difficult to reconcile with independent uptake of pre-existing small nanoparticles, which would be expected to exhibit a more random spatial distribution. Instead, these morphological features are more consistent with *in situ* fragmentation of longer nanowires into shorter segments that remain locally associated following breakage.

Notably, the Au nanowires in the initial suspension span lengths from tens of nanometres to several micrometres (Fig. 1B), whereas within plant tissues they are predominantly observed as fragmented segments ranging from a few nanometres to several hundred nanometres in length, while their diameters remain largely unchanged. This pronounced shift in length distribution, without a corresponding reduction in diameter, further supports a fragmentation process rather than selective uptake alone. Although this observation appears inconsistent with the commonly cited plant size-exclusion limit of ~20 nm,[46] previous studies have demonstrated that nanoparticles spanning a broad size range (*e.g.*, TiO_2, 4–100 nm) can penetrate the cuticle by locally disrupting cuticular waxes, as evidenced by TEM-EDX, cuticle and cell wall damage, and ToF-SIMS depth profiling showing nanoparticle accumulation beneath the cuticle.[8]

We therefore propose that the observed Au nanowire segments access and translocate within plant tissues by locally bypassing or altering the cuticular barrier. Selective uptake of smaller nanostructures may contribute to this process but is unlikely to be the dominant mechanism. Instead, fragmentation of longer nanowires during uptake and translocation provides a more consistent explanation for the increased abundance, spatial organization, and size distribution of Au nanostructures observed within leaves, stems, and roots.

Nanowires are inherently susceptible to fragmentation due to Plateau–Rayleigh instability,[56] and this process may be further promoted by mechanical stress, chemical interactions, and biological activity.[57,58] During translocation, nanowires may experience bending or shear forces within plant tissues, leading to breakage.[59] Additionally, interactions with the plant's internal biochemical environment, including enzymatic activity and reactive oxygen species, may further facilitate nanowire degradation.[58,60,61]

Fig. 5H and I and S7A–C suggest that Au spherical nanocarriers, unlike the wire-shaped ones, translocate through a 'highway' within plant leaves, corresponding to the apoplastic space, such as the network of cell walls and intercellular spaces, facilitating more efficient transport. Several factors may contribute to the formation of such a pathway for spherical nanocarriers. Their smaller, compact shape could facilitate more uniform and passive distribution through the plant's vascular system, particularly in the apoplast and fluid-conducting tissues like the phloem. The spherical geometry may allow them to avoid clogging or becoming trapped in narrow spaces, as they can easily adapt to the flow dynamics in these channels. Furthermore, their uniform surface charge distribution might enhance interaction with water-conducting pathways, leading to smoother, less restricted movement. Additionally, the plant's uptake mechanisms may favour spherical nanocarriers due to their more compatible size and shape for vesicular transport or pore diffusion. In contrast, wire-shaped nanocarriers, due to their elongated form and increased surface area, may experience more physical obstruction and resistance as they attempt to navigate through complex plant structures.

To determine whether Cu was successfully delivered or remained associated with the Au nanocarriers, an EDX line scan across the wire nanocarrier clusters at the plant–resin interface was conducted, as shown in Fig. S8. The EDX profile reveals a strong signal for Au, a weaker signal for Cu, and even fainter signals for U, from uranyl acetate staining, and P, which originates from the plant's natural phosphorus metabolism, all within the Au wire nanocarriers. This suggests that Cu delivery may be incomplete or still in progress. After uptake, it is possible that the micronutrient Cu is adsorbed and gradually delivered to different parts of the plant.

Although Fig. 5A–F show that most nanocarriers remain within the cuticle, some nanocarriers were observed penetrating the cell wall and staying inside cells (Fig. S7E) of plant leaves. In Fig. S7D, although most nanocarriers translocate the cuticle layer of a plant leaf, some, approximately 50 nm or smaller as indicated by the dotted yellow circle, appears to be in the process of penetrating the cell wall. The number of penetrating nanocarriers is considerably lower than those traveling along the cuticle, suggesting that movement along the cuticle is less restricted compared to cell wall penetration. In this study, we observed that only elongated nanocarriers penetrated the cuticle, while spherical ones did not. This observation may relate to the proposed rotation and internalization mechanisms.[12] It suggests that wire-shaped nanocarriers primarily enter the plant through wounds or openings such as stomata, which significantly restricts their overall uptake and reduces the yield of internalization.

Interestingly, it would be valuable to investigate whether these penetrating nanocarriers follow a rotation-mediated mechanism, as suggested in previous studies.[5] This research indicated that elongated nanocarriers might traverse plant cell walls through a rotation process that orients them favourably at acute angles relative to the plane of the cell wall. Such orientation could be induced by local changes in fluid dynamics resulting from applied external forces.

Fig. S7E and inset show another region of the plant leaf. Several organelles with stacked membrane structures, are identified as grana, within the chloroplasts. These structures are crucial for photosynthesis and are abundant in mesophyll

cells. The well-defined chloroplasts, with their typical grana structure, signify healthy mesophyll cells. Small, distinct particles observed in the cellular matrix and chloroplasts are identified as nanocarriers based on their size, shape, and distribution. The presence of nanocarriers inside mesophyll cells indicates successfully uptake and distribution through the tissue. In plant leaves, spherical nanocarriers maintain their shape as discrete dots, while wire-shaped nanocarriers often appear fragmented, due to the mechanical stress or chemical processes during uptake or translocation. Both types are found in the cuticle, with wire-shaped nanocarriers fragmenting as they pass through this barrier. Inside the leaf, fragments of wire nanocarriers, along with intact spherical ones, are present within cell walls and mesophyll cells, but only spherical nanocarriers exhibit "highway-like" translocation *via* the apoplastic pathway. A schematic of this distribution is shown in Fig. 5G.

Fig. 6 illustrates the localization and distribution of spherical and wire-shaped Au nanocarriers within plant stems. Fig. 6A–C, with increasing magnification, reveals Au spherical nanocarriers within the phloem of the eggplant stem, including structures such as sieve plates, sieve elements, and parenchyma cells. The proximity of the Au nanocarriers to the phloem sieve plates implies that their translocation is facilitated by the flow of phloem sap. While the majority of spherical nanocarriers retain their original morphology (Fig. 6C), some particles exhibit irregular shapes and agglomerated structures.

These morphological changes are unlikely to arise from complete dissolution of metallic gold, which would require highly oxidative and complexing conditions not expected in planta. Instead, they are more plausibly attributed to surface-level restructuring processes, such as partial oxidative etching, ligand-mediated surface atom detachment, and subsequent re-agglomeration during uptake and translocation. The complex biochemical environment of plant tissues—including organic acids, thiol-containing compounds, and reactive oxygen species—may facilitate such surface modifications without full dissolution of the Au core. Together with the observed fragmentation of Au nanowires (Fig. 5 and inset and 6E), these results suggest that Au nanocarriers undergo morphology evolution during plant uptake and transport, driven by mechanical, chemical, and biological interactions within plant tissues. The inset in Fig. 6C confirms the presence of Au nanocarrier clusters through EDX mapping.

Fig. 6D–F present HAADF-STEM images of Au wire nanocarriers within the eggplant stem. In Fig. 6D, regions containing wire-shaped nanocarriers are highlighted by green and purple dashed squares and are magnified in Fig. 6E and F. These images reveal fragmented Au nanocarriers located within stem microstructures, including the cell wall and sieve elements, consistent with the nanowire fragmentation behaviour described above (Fig. 5).

Notably, fragmented nanowires appear to translocate along cell walls and converge or diverge at cell junctions, such as plasmodesmata, as shown in Fig. 6F. The presence of wire-shaped nanocarriers near plasmodesmata, further highlighted in the green dashed region of Fig. 6D, suggests that elongated nanocarriers or their fragments may access symplastic pathways under certain conditions. The inset of Fig. 6F confirms the presence of Au within these wire-shaped nanostructures by STEM-EDX analysis.

Fig. 6H highlights the resin and cuticle of a plant stem, where spherical nanocarriers can be observed within the cuticle layer (see Fig. 6H and S9). As shown in the yellow-dotted region of Fig. 6H, many spherical nanocarriers are present. Some are located at the interface between the cuticle and resin, while others remain embedded within the cuticle. The

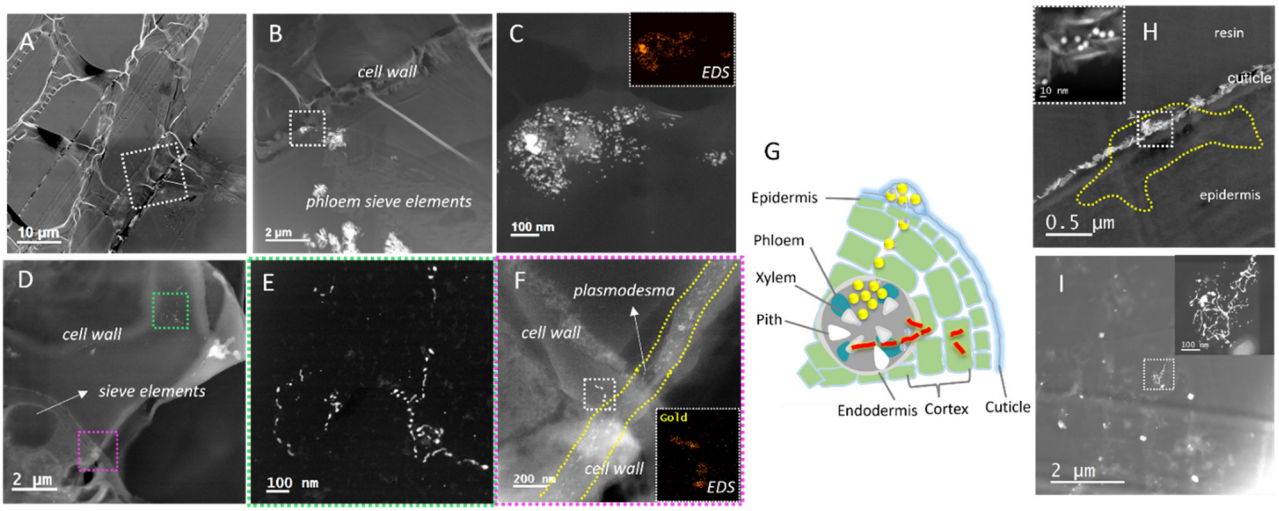

Fig. 6 HAADF-STEM images of Au nanocarriers in eggplant stems: (A–C, H) show spherical nanocarriers, and (D–F, I) show wire-shaped nanocarriers. (G) A schematic drawing illustrating the distribution of nanocarriers in plant stems. White dotted boxes in (A, B, F, H, and I) are magnified to highlight regions containing nanocarriers, while yellow dotted lines mark areas with nanocarriers. Green and purple dotted boxes in (D) indicate regions of interest, which are further magnified in (E) and (F).

nanocarriers at the interface are wrapped in waxes, cutin, or polysaccharides from the cuticle.

For spherical nanocarriers retained within the cuticle, we propose that these particles are undergoing post-translocation re-deposition toward the outer stem surface, consistent with plant exclusion of non-essential elements. Importantly, in this study, only spherical nanocarriers were observed at or near the outer cuticle of the stem following uptake and internal transport, whereas wire-shaped nanocarriers were not detected undergoing a similar re-deposition process. This contrast highlights a strong morphology dependence in nanocarrier fate within plant tissues. While elongated nanocarriers appear to fragment and disperse within internal tissues—particularly near sieve elements and plasmodesmata—spherical nanocarriers remain structurally intact and are more readily excluded toward the cuticle. The absence of wire-shaped nanocarriers at the stem cuticle may be attributed to their elongated geometry, which could hinder their ability to migrate through dense cellular architectures or traverse toward the cuticular barrier due to increased friction, entanglement, or mechanical constraints.

Fig. 6I further illustrates the presence of nanocarriers within stem cells, showing a heterogeneous population with a wide range of sizes and morphologies. Spherical nanocarriers tend to remain clustered, whereas wire-shaped nanocarriers are predominantly observed as fragmented and more widely dispersed structures. Overall, both nanocarrier types are primarily localized near sieve elements of the stem, as summarized schematically in Fig. 6G, supporting phloem-associated transport following foliar uptake. Together, these observations indicate that Au nanocarriers undergo pronounced morphology evolution during plant uptake and transport, driven by mechanical, chemical, and biological interactions within plant tissues, with size and shape playing a critical role in fragmentation, transport pathways, and exclusion behaviour.

Fig. 7 and S10 show the distribution of spherical and wire nanocarriers in transverse sections of eggplant roots. The yellow dotted lines in the images indicate the locations where Au nanocarriers are present. Fig. 7A–C reveal that Au spherical nanocarriers are primarily distributed around the cell walls, exhibiting morphologies ranging from isolated spherical particles to agglomerated and irregular particles. The EDX map inset in Fig. 7C confirms the presence of Au spherical nanocarriers. The interaction between nanoparticles and plants is complex, influenced by factors such as biomolecules (enzymes and phytochemicals), biochemical environment (pH, presence of ligands, and metal ion concentrations), transport paths (passive diffusion, active transport, and endocytosis), and nanoparticle surface properties (charge and coating).[10,62–66] These variables can cause changes in nanocarrier morphology. Transformation of nanocarriers, such as nanowires, predominates within cell wall and intracellular compartments, where mechanical constraints, enzymatic activity, and pH variations are higher. Regions associated with vascular transport may further promote transformation due to pressure and flow, whereas extracellular or low-activity regions may experience limited structural change. Further research is needed to understand the factors driving these transformations and the parameters controlling nanocarrier translocation.

Fig. 7D–F show fragmented Au nanocarriers located at the interface between the epidermis and resin of root samples. This localization suggests that, upon reaching the root, nanocarriers are preferentially retained within epidermal cells or root hairs, consistent with exclusion of non-essential elements. Fig. 7H and I further show the presence of nanocarriers in the intercellular space and inside root cells, where both their morphology and size are altered. These observations are consistent with confocal fluorescence imaging (Fig. 3D), which confirms the presence of Au nanocarriers in roots following foliar application.

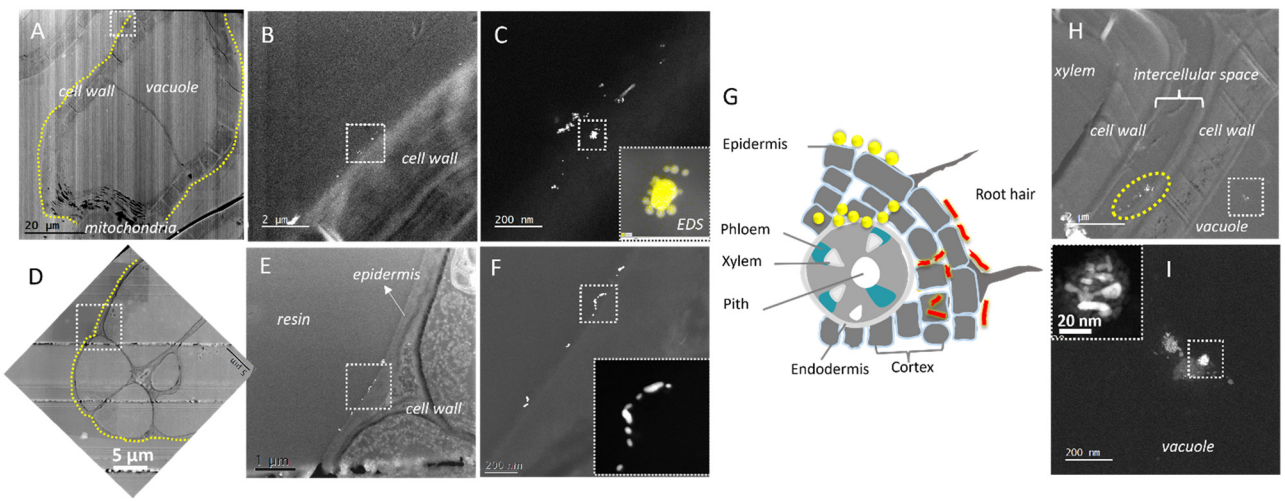

Fig. 7 HAADF-STEM images of (A–C) Au spherical and (D–F, H and I) wire nanocarriers in eggplant roots. (G) A schematic illustrates the distribution of the nanocarriers. Yellow dotted lines indicate regions containing nanocarriers, and white dotted boxes highlight areas of interest. The inset EDX map confirms the presence of Au nanocarriers. The region within the dotted box in (H) is magnified in (I) and further magnified in the inset in (I).

Notably, Au nanocarriers are consistently observed at the root surface and epidermal interfaces, regardless of their initial morphology, suggesting biologically regulated immobilization or exclusion rather than direct root exposure. This interpretation is supported by prior work by Avellan *et al.*,[5] who demonstrated that foliar-applied Au nanoparticles can be translocated to roots and subsequently exuded into the rhizosphere, indicating that roots can act as terminal sinks or exclusion sites for non-essential nanomaterials. The presence of Au nanocarriers at the root interface in this study is therefore consistent with long-distance transport following foliar uptake and subsequent exclusion at the root level.

Fig. 7G is a schematic illustration of nanocarriers in plant roots. Both spherical and wire-shaped nanocarriers are predominantly associated with cell walls; spherical nanocarriers tend to retain their morphology and aggregate, whereas wire-shaped nanocarriers are more prone to fragmentation and dispersion. Together, these results indicate that nanocarrier size and shape play a key role in determining transport, transformation, and exclusion behaviour within root tissues.

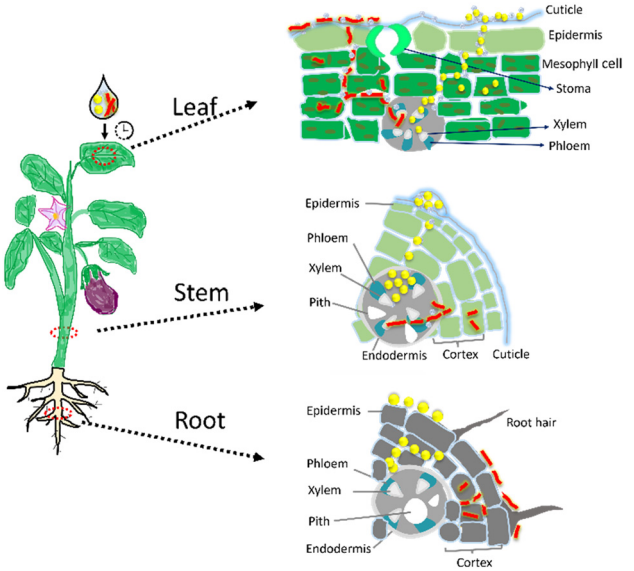

Scheme 2 Schematic representation of the uptake and translocation of Au nanocarriers from the plant leaf to the stem and then to the root.

3.3. Mechanism

The interaction between nanoparticles and plants is a complex process influenced by nanoparticle properties, plant physiology, and environmental factors.[67] Upon foliar application, nanocarriers adhere to the leaf surface *via* electrostatic, van der Waals, or chemical interactions.[62] They are then taken up through various pathways, including trichomes, microscopic wounds, or possibly endocytosis, as noted in previous studies,[5,68] although they are not directly resolved here.

The presence of Au nanocarriers in leaves, stems, and roots demonstrates effective internal redistribution following foliar exposure (see Scheme 2). In leaves, spherical nanocarriers are predominantly localised along cell walls and intercellular spaces, consistent with transport through interconnected apoplastic pathways (highways). Such transport is influenced by nanocarrier shape and local physicochemical conditions. Wire-shaped nanocarriers are frequently observed in fragmented forms across multiple plant compartments. Given the low fraction of nanospheres in the initial suspension, this observation indicates in planta transformation rather than selective uptake of pre-existing fragments. While the specific drivers of fragmentation cannot be conclusively identified, the observations are consistent with mechanical constraints and biochemical interactions within plant tissues.

Nanocarriers detected near phloem-associated structures in stems support long-distance redistribution following foliar uptake. As the stem surface was not directly exposed during application, their presence is attributed to internal transport rather than external contamination. At the root level, nanocarriers are predominantly localised in epidermal layers, cell walls, and intercellular spaces, suggesting that roots act as terminal compartments for the accumulation or exclusion of non-essential elements.

Overall, the results indicate a morphology-dependent influence on nanocarrier transformation and spatial distribution in planta. Spherical nanocarriers largely retain their morphology during transport, whereas wire-shaped nanocarriers undergo extensive fragmentation. These findings provide an experimentally supported framework for morphology-dependent behaviour, while recognising that the underlying molecular transport mechanisms require further investigation.

4. Conclusions

This study investigated the interaction of Au nanocarriers with eggplants, focusing on their uptake, translocation, and morphological changes. We designed and synthesized uniform hydrophilic β-CD polymer capped-Au nanospheres and nanowires, further loaded with Cu–EDTA. Following foliar application, we monitored the behaviour of nanocarriers using various analytical techniques. By employing high-resolution STEM-EDX for spatial and chemical mapping and supported by complementary techniques including ICP-OEC and confocal microscopy, we obtained direct evidence for several morphology-dependent behaviours.

Our key experimental findings are: (1) both spherical and wire-shaped nanocarriers were taken up and systemically translocated, with primary accumulation in treated leaves but detectable presence in stems and roots. (2) Wire-shaped nanocarriers underwent significant morphological transformation, including fragmentation and the formation of large clusters during translocation, whereas spherical carriers largely maintained their discrete form. (3) Correlative microscopy localised nanocarriers along pathways consistent with apoplastic transport, suggesting a "highway" through intercellular spaces that appears more accessible to spherical morphologies. (4) At the root level, nanocarriers of both types

were found accumulated at the tissue periphery, indicating a potential point of exclusion or sequestration.

Based on these observations, we propose a model where nanocarrier morphology critically influences the post-uptake fate: spherical carriers translocate more readily *via* apoplastic corridors (highways), while high-aspect-ratio wires are prone to physical breakdown and aggregation. These insights, derived from direct nano-scale imaging, advance the understanding of shape-dependent nanoparticle transport in plants. They highlight the importance of design principles for nanocarriers intended for foliar delivery, where optimizing shape can modulate mobility, stability, and final distribution. However, the applicability of these findings is limited to the eggplant model system used herein. Future work should expand these findings to other plant species and exposure scenarios to assess their broader applicability.

Author contributions

L. F. X. and Y. M. L. conceived and designed the project. L. F. X. performed the experiments and was responsible for data curation, validation, visualization, investigation, and drafting the original manuscript. Y. M. W., A. M. Q., Y. Y. T., and C. B. contributed to materials characterization and participated in reviewing and editing the manuscript. Y. M. L. provided resources and contributed to project administration, supervision, validation, and manuscript review and editing.

Conflicts of interest

There are no conflicts of interest to declare.

Data availability

All data supporting the findings of this study are included within the manuscript and the accompanying supplementary information (SI).

Supplementary information, including a table and figures, is available. See DOI: https://doi.org/10.1039/d5en00920k.

Acknowledgements

We acknowledge Prof Alexander Ludwig and Mr Ronald B. Y. Kan for their help and discussion during the project. Y. M. L. is grateful for funding support from the Ministry of Education under an AcRF Tier 1 thematic grant (RT09/20) and AcRF Tier 1 grant (RG13/24).

References

1 D. Mittal, G. Kaur, P. Singh, K. Yadav and S. A. Ali, Nanoparticle-based sustainable agriculture and food science: recent advances and future outlook, *Front. Nanotechnol.*, 2020, **2**, 579954.
2 Y. Shang, M. K. Hasan, G. J. Ahammed, M. Li, H. Yin and J. Zhou, Applications of nanotechnology in plant growth and crop protection: a review, *Molecules*, 2019, **24**, 2558.
3 P. Zhang, Z. Guo, S. Ullah, G. Melagraki, A. Afantitis and I. Lynch, Nanotechnology and artificial intelligence to enable sustainable and precision agriculture, *Nat. Plants*, 2021, **7**, 864–876.
4 L. Xi, M. Zhang, L. Zhang, T. T. S. Lew and Y. M. Lam, Novel materials for urban farming, *Adv. Mater.*, 2022, **34**, 2105009.
5 A. Avellan, J. Yun, Y. Zhang, E. Spielman-Sun, J. M. Unrine, J. Thieme, J. Li, E. Lombi, G. Bland and G. V. Lowry, Nanoparticle size and coating chemistry control foliar uptake pathways, translocation, and leaf-to-rhizosphere transport in wheat, *ACS Nano*, 2019, **13**, 5291–5305.
6 S. Wang, J. Lv, J. Ma and S. Zhang, Cellular internalization and intracellular biotransformation of silver nanoparticles in Chlamydomonas reinhardtii, *Nanotoxicology*, 2016, **10**, 1129–1135.
7 H. Kohay, J. Wielinski, J. Reiser, L. A. Perkins, K. Ristroph, J. P. Giraldo and G. V. Lowry, Nanocarrier foliar uptake pathways affect delivery of active agents and plant physiological response, *Environ. Sci.: Nano*, 2025, **12**, 660–674.
8 C. Larue, H. Castillo-Michel, S. Sobanska, N. Trcera, S. Sorieul, L. Cécillon, L. Ouerdane, S. Legros and G. Sarret, Fate of pristine TiO_2 nanoparticles and aged paint-containing TiO_2 nanoparticles in lettuce crop after foliar exposure, *J. Hazard. Mater.*, 2014, **273**, 17–26.
9 R. Bala, A. Kalia and S. S. Dhaliwal, Evaluation of efficacy of ZnO nanoparticles as remedial zinc nanofertilizer for rice, *J. Soil Sci. Plant Nutr.*, 2019, **19**, 379–389.
10 P. Hu, J. An, M. M. Faulkner, H. Wu, Z. Li, X. Tian and J. P. Giraldo, Nanoparticle charge and size control foliar delivery efficiency to plant cells and organelles, *ACS Nano*, 2020, **14**, 7970–7986.
11 R. Raliya, C. Franke, S. Chavalmane, R. Nair, N. Reed and P. Biswas, Quantitative understanding of nanoparticle uptake in watermelon plants, *Front. Plant Sci.*, 2016, **7**, 1288.
12 H. Zhang, N. S. Goh, J. W. Wang, R. L. Pinals, E. Gonzalez-Grandio, G. S. Demirer, S. Butrus, S. C. Fakra, A. Del Rio Flores, R. Zhai, B. Zhao, S. J. Park and M. P. Landry, Nanoparticle cellular internalization is not required for RNA delivery to mature plant leaves, *Nat. Nanotechnol.*, 2022, **17**, 197–205.
13 J. Pauli, M. Grabolle, R. Brehm, M. Spieles, F. M. Hamann, M. Wenzel, I. Hilger and U. Resch-Genger, Suitable labels for molecular imaging – influence of dye structure and hydrophilicity on the spectroscopic properties of IgG conjugates, *Bioconjugate Chem.*, 2011, **22**, 1298–1308.
14 V. R. Myers, What is foliar application for horticultural plants?, The Spruce, https://www.thespruce.com/what-is-a-foliar-application-3269801, (accessed 16 October 2021).
15 D. Oosterhuis, Foliar fertilization: mechanisms and magnitude of nutrient uptake, *Proceedings of the Fluid Forum*, Phoenix, AZ, 15–17 February 2009.
16 B. Aswathy, G. S. Avadhani, S. Suji and G. Sony, Synthesis of β-cyclodextrin functionalized gold nanoparticles for the selective detection of Pb^{2+} ions from aqueous solution, *Front. Mater. Sci.*, 2012, **6**, 168–175.
17 Y. Huang, D. Li and J. Li, β-Cyclodextrin controlled assembling nanostructures from gold nanoparticles to gold nanowires, *Chem. Phys. Lett.*, 2004, **389**, 14–18.

18 I. Santana, H. Wu, P. Hu and J. P. Giraldo, Targeted delivery of nanomaterials with chemical cargoes in plants enabled by a biorecognition motif, *Nat. Commun.*, 2020, **11**, 2045.
19 Y. Li, J. Qi, Q. Gao, C. He, J. Gu, Z. Xie, Z. Li and H. Wu, Plants primed with CeO_2 nanoparticles increased DNA methylation level to convey transgenerational salinity tolerance, *Plant Nano Biol.*, 2025, **14**, 100214.
20 C. P. Han and H. B. Li, Novel β-cyclodextrin modified quantum dots as fluorescent probes for polycyclic aromatic hydrocarbons, *Chin. Chem. Lett.*, 2008, **19**, 215–218.
21 C. Park, H. Youn, H. Kim, T. Noh, Y. H. Kook, E. T. Oh, H. J. Park and C. Kim, Cyclodextrin-covered gold nanoparticles for targeted delivery of an anti-cancer drug, *J. Mater. Chem.*, 2009, **19**, 2310–2315.
22 X. Ai, L. Niu, Y. Li, F. Yang and X. Su, A novel β-cyclodextrin-QDs optical biosensor for the determination of amantadine and its application in cell imaging, *Talanta*, 2012, **99**, 409–414.
23 N. M. Y. Zhang, M. Qi, Z. Wang, Z. Wang, M. Chen, K. Li, P. Shum and L. Wei, One-step synthesis of cyclodextrin-capped gold nanoparticles for ultra-sensitive and highly integrated plasmonic biosensors, *Sens. Actuators, B*, 2019, **286**, 429–436.
24 S. Daoud-Mahammed, J. L. Grossiord, T. Bergua, C. Amiel, P. Couvreur and R. Gref, Self-assembling cyclodextrin-based hydrogels for the sustained delivery of hydrophobic drugs, *J. Biomed. Mater. Res., Part A*, 2008, **86**, 736–748.
25 G. Salzano, J. Wankar, S. Ottani, B. Villemagne, A. R. Baulard, N. Willand, P. Brodin, I. Manet and R. Gref, Cyclodextrin-based nanocarriers containing a synergic drug combination: a potential formulation for pulmonary administration of antitubercular drugs, *Int. J. Pharm.*, 2017, **531**, 577–587.
26 T. Huang, F. Meng and L. Qi, Facile synthesis and one-dimensional assembly of cyclodextrin-capped gold nanoparticles and their applications in catalysis and surface-enhanced Raman scattering, *J. Phys. Chem. C*, 2009, **113**, 13636–13642.
27 Y. S. Pestovsky and A. Martínez-Antonio, Synthesis of gold nanoparticles by tetrachloroaurate reduction with cyclodextrins, *Quim. Nova*, 2018, **41**, 926–932.
28 D. A. Körpe and S. Aras, Evaluation of copper-induced stress on eggplant (*Solanum melongena* L.) seedlings at the molecular and population levels by use of various biomarkers, *Mutat. Res., Genet. Toxicol. Environ. Mutagen.*, 2011, **719**, 29–34.
29 K. Iwasaki and E. Takahashi, Effects of charge characteristics of Cu-chelates on the Cu uptake from solution by Italian ryegrass and red clover, *Soil Sci. Plant Nutr.*, 1989, **35**, 145–150.
30 T. K. Udeigwe, M. B. Eichmann, M. C. Menkiti and N. Y. O. Kusi, Examining the fixation kinetics of chelated and non-chelated copper and the applications to micronutrient management in semiarid alkaline soils, *Solid Earth*, 2016, **7**, 311–321.
31 L. M. Skjolding, L. v. G. Jørgensen, K. S. Dyhr, C. J. Köppl, U. S. McKnight, P. Bauer-Gottwein, P. Mayer, P. L. Bjerg and A. Baun, Assessing the aquatic toxicity and environmental safety of tracer compounds Rhodamine B and Rhodamine WT, *Water Res.*, 2021, **197**, 117109.
32 P. C. Naha, P. Chhour and D. P. Cormode, Systematic in vitro toxicological screening of gold nanoparticles designed for nanomedicine applications, *Toxicol. In Vitro*, 2015, **29**, 1445–1453.
33 A. J. Mieszawska, W. J. M. Mulder, Z. A. Fayad and D. P. Cormode, Multifunctional gold nanoparticles for diagnosis and therapy of disease, *Mol. Pharmaceutics*, 2013, **10**, 831–847.
34 S. A. Bansal, V. Kumar, J. Karimi, A. P. Singh and S. Kumar, Role of gold nanoparticles in advanced biomedical applications, *Nanoscale Adv.*, 2020, **2**, 3764–3787.
35 V.-D. Doan, *et al.*, Biosynthesis of silver and gold nanoparticles using aqueous extract of *Codonopsis pilosula* roots for antibacterial and catalytic applications, *J. Nanomater.*, 2020, **2020**, 8492016.
36 H. Liu, X. Liu, Y. Yu, W. Yang, J. Li, M. Feng and H. Li, Bifunctional networked Ag/AgPd core/shell nanowires for highly efficient dehydrogenation of formic acid and subsequent reduction of nitrate and nitrite in water, *J. Mater. Chem. A*, 2018, **6**, 4611–4616.
37 M. Behera and S. Ram, Synthesis and characterization of core–shell gold nanoparticles with poly(vinyl pyrrolidone) from a new precursor salt, *Appl. Nanosci.*, 2013, **3**, 83–87.
38 G. W. Lu and P. Gao, Non-invasive drug delivery systems, in *Handbook of Non-Invasive Drug Delivery Systems*, ed. V. S. Kulkarni, William Andrew Publishing, Boston, 2010, pp. 59–94.
39 L. F. Xi, C. Schwanke, K. M. Lange and M. Risch, In situ ATR infrared study of cobalt–borate water oxidation catalysts, *Mater. Sci. Forum*, 2020, **998**, 123–133.
40 D. Peak, Surface complexation modeling, in *Reference Module in Earth Systems and Environmental Sciences*, Elsevier, 2013.
41 M. Raoov, S. Mohamad and M. R. Abas, Synthesis and characterization of β-cyclodextrin functionalized ionic liquid polymer as a macroporous material for the removal of phenols and As(V), *Int. J. Mol. Sci.*, 2014, **15**, 100–119.
42 D. T. Sawyer and P. J. Paulsen, Properties and infrared spectra of ethylenediaminetetraacetic acid complexes. II. Chelates of divalent ions, *J. Am. Chem. Soc.*, 1959, **81**, 816–820.
43 V. Ramalakshmi and J. Balavijayalakshmi, Influence of gold nanoparticle concentration on polymer functionalized reduced graphene nanosheets and its electrochemical sensing performance, *Mater. Res. Express*, 2019, **6**, 075013.
44 F. Zhao, E. Repo, D. Yin, Y. Meng, S. Jafari and M. Sillanpää, EDTA-cross-linked β-cyclodextrin: an environmentally friendly bifunctional adsorbent for simultaneous adsorption of metals and cationic dyes, *Environ. Sci. Technol.*, 2015, **49**, 10570–10580.
45 J. Ou, Y. Hu, L. Huang, R. Zhang, T. Xu and J. Zhao, pH-sensitive nanocarriers for *Ganoderma applanatum* polysaccharide release via host–guest interactions, *J. Mater. Sci.*, 2018, **53**, 7963–7975.
46 E. Etxeberria, P. Gonzalez, P. Bhattacharya, P. Sharma and P. C. Ke, Determining the size exclusion for nanoparticles in citrus leaves, *Hortscience*, 2016, **51**, 732–737.
47 T. Eichert, A. Kurtz, U. Steiner and H. E. Goldbach, Size exclusion limits and lateral heterogeneity of the stomatal foliar uptake pathway for aqueous solutes and water-suspended nanoparticles, *Physiol. Plant.*, 2008, **134**, 151–160.

48 N. K. Fageria, M. P. B. Filho, A. Moreira and C. M. Guimarães, Foliar fertilization of crop plants, *J. Plant Nutr.*, 2009, **32**, 1044–1064.
49 D. A. Wait, *Lecture 11: Transport in Plant*, http://courses.missouristate.edu/alexanderwait/notes/lecture%20notes/lecture%2011.htm, (accessed 16th October, 2021).
50 H. Malhotra, R. Pandey, S. Sharma and P. S. Bindraban, Foliar fertilization: possible routes of iron transport from leaf surface to cell organelles, *Arch. Agron. Soil Sci.*, 2019, **66**, 279–300.
51 J. Zhang and P. X. Ma, Cyclodextrin-based supramolecular systems for drug delivery: recent progress and future perspective, *Adv. Drug Delivery Rev.*, 2013, **65**, 1215–1233.
52 S. Chen, H. Diekmann, D. Janz and A. Polle, Quantitative X-ray elemental imaging in plant materials at the subcellular level with a transmission electron microscope: applications and limitations, *Materials*, 2014, **7**, 3160–3175.
53 P. Guzman, V. Fernandez, M. Khayet, M. L. Garcia, A. Fernandez and L. Gil, Ultrastructure of plant leaf cuticles in relation to sample preparation as observed by transmission electron microscopy, *Sci. World J.*, 2014, **2014**, 963921.
54 C. Ziv, Z. Zhao, Y. G. Gao and Y. Xia, Multifunctional roles of plant cuticle during plant–pathogen interactions, *Front. Plant Sci.*, 2018, **9**, 1088.
55 L. Valerga, M. Darré, M. J. Zaro, A. Arambarri, A. R. Vicente, M. L. Lemoine and A. Concellón, Micro-structural and quality changes in growing dark-purple eggplant (*Solanum melongena* L.) as affected by the harvest season, *Sci. Hortic.*, 2019, **244**, 22–30.
56 S. Bettscheider, T. Kraus and N. A. Fleck, On the geometric stability of an inorganic nanowire and an organic ligand shell, *J. Mech. Phys. Solids*, 2019, **123**, 3–19.
57 T. Isah, Stress and defense responses in plant secondary metabolites production, *Biol. Res.*, 2019, **52**, 39.
58 H. Wu, N. Tito and J. P. Giraldo, Anionic cerium oxide nanoparticles protect plant photosynthesis from abiotic stress by scavenging reactive oxygen species, *ACS Nano*, 2017, **11**, 11283–11297.
59 *Advanced Materials for Agriculture, Food, and Environmental Safety*, ed. A. Tiwari and M. Syväjärvi, John Wiley & Sons, Inc., Hoboken, NJ, 2014.
60 A. Karny, A. Zinger, A. Kajal, J. Shainsky-Roitman and A. Schroeder, Therapeutic nanoparticles penetrate leaves and deliver nutrients to agricultural crops, *Sci. Rep.*, 2018, **8**, 7589.
61 S. Behzadi, V. Serpooshan, W. Tao, M. A. Hamaly, M. Y. Alkawareek, E. C. Dreaden, D. Brown, A. M. Alkilany, O. C. Farokhzad and M. Mahmoudi, Cellular uptake of nanoparticles: journey inside the cell, *Chem. Soc. Rev.*, 2017, **46**, 4218–4244.
62 M. R. Khan, V. Adam, T. F. Rizvi, B. Zhang, F. Ahamad, I. Jośko, Y. Zhu, M. Yang and C. Mao, Nanoparticle–plant interactions: two-way traffic, *Small*, 2019, **15**, 1901794.
63 P. Wang, E. Lombi, F. J. Zhao and P. M. Kopittke, Nanotechnology: a new opportunity in plant sciences, *Trends Plant Sci.*, 2016, **21**, 699–712.
64 Y. Su, V. Ashworth, C. Kim, A. S. Adeleye, P. Rolshausen, C. Roper, J. White and D. Jassby, Delivery, uptake, fate, and transport of engineered nanoparticles in plants: a critical review and data analysis, *Environ. Sci.: Nano*, 2019, **6**, 2311–2331.
65 N. S. Feichtmeier, P. Walther and K. Leopold, Uptake, effects, and regeneration of barley plants exposed to gold nanoparticles, *Environ. Sci. Pollut. Res.*, 2015, **22**, 8549–8558.
66 G. Zhai, K. S. Walters, D. W. Peate, P. J. J. Alvarez and J. L. Schnoor, Transport of gold nanoparticles through plasmodesmata and precipitation of gold ions in woody poplar, *Environ. Sci. Technol. Lett.*, 2014, **1**, 146–151.
67 A. Pérez-de-Luque, Interaction of nanomaterials with plants: what do we need for real applications in agriculture?, *Front. Environ. Sci.*, 2017, **5**, 12.
68 P. P. Nadiminti, Y. D. Dong, C. Sayer, P. Hay, J. E. Rookes, B. J. Boyd and D. M. Cahill, Nanostructured liquid crystalline particles as an alternative delivery vehicle for plant agrochemicals, *ACS Appl. Mater. Interfaces*, 2013, **5**, 1818–1826.

